1 **Impacts of Three Gorges Dam's operation on spatial-temporal**

2 **patterns of tide-river dynamics in the Yangtze River estuary, China**

3 Huayang Cai[1,2,3,4], Xianyi Zhang[1,2,3], Min Zhang[5,*], Leicheng Guo[4], Feng Liu[1,2,3],
4 Qingshu Yang[1,2,3]
5
6 *1. Institute of Estuarine and Coastal Research, School of Marine Engineering and*
7 *Technology, Sun Yat-sen University, Guangzhou, China*
8 *2. Guangdong Provincial Engineering Research Center of Coasts, Islands and Reefs,*
9 *Guangzhou, China*
10 *3. Southern Marine Science and Engineering Guangdong Laboratory (Zhuhai),*
11 *Zhuhai, China*
12 *4. State Key Laboratory of Estuarine and Coastal Research, East China Normal*
13 *University, Shanghai, China*
14 *5. Shanghai Normal University, School of Environmental and Geographical Sciences,*
15 *Shanghai, China*
16 **Corresponding author:** Min Zhang
17 **Corresponding author's E-mail:** zhangmin@shnu.edu.cn

19 **Key points**

20 1.  Impacts of TGD operation on tide-river dynamics are quantified using an analytical

21     model.

22 2.  The strongest impacts occurred during autumn and winter due to the seasonal

23     freshwater regulation by TGD.

24 3.  The alteration of tide-river dynamics may exert considerable impacts on sustainable

25     water resource management in dam-controlled estuaries.

**Abstract**

The Three Gorges Dam (TGD), located in the mainstream of the Yangtze River, is the world's largest hydroelectric station in terms of installed power capacity. It was demonstrated that the TGD had caused considerable modifications in the downstream freshwater discharge due to its seasonal operation mode of multiple utilisation for flood control, irrigation, and power generation. To understand the impacts of the freshwater regulation of TGD, an analytical model is adopted to explore how the operation of TGD may affect the spatial-temporal patterns of tide-river dynamics in the Yangtze River estuary. We evaluated the effect of TGD by comparing the changes in major tide-river dynamics in the post-TGD period (2003–2014) with those in the pre-TGD period (1979–1984). The results indicate that the strongest impacts occurred during the autumn and winter, corresponding to a substantial reduction in freshwater discharge during the wet-to-dry transition period and slightly increased discharge during the dry season. The underlying mechanism leading to changes in the tide-river dynamics lies in the alteration of freshwater discharge, while the impact of geometric change is minimal. Overall, the results suggest that the spatial-temporal pattern of tide-river dynamics is sensitive to the freshwater regulation of the TGD, so that the ecosystem function of the estuary may undergo profound disturbances. The results obtained from this study can be used to set scientific guidelines for water resource management (e.g. navigation, flood control, salt intrusion) in dam-controlled estuarine systems.

**Key words:** seasonal freshwater regulation, Three Gorges Dam, analytical model, tide-river dynamics, Yangtze River estuary

## 1. Introduction

Estuaries are transition zones where river meets ocean (Savenije, 2012). Tide-river interactions, a result of both hydrologic drivers and geomorphic constraints, are highly dynamic in estuaries (Buschman et al., 2009; Sassi and Hoitink, 2013; Guo et al., 2015; Cai et al., 2016; Hoitink and Jay, 2016; Hoitink et al., 2017; Du et al., 2018). In natural conditions, they usually experience a wide range of temporal variations, in timescale ranging from a fortnight to season (e.g. Zhang et al., 2018). Human intervention, such as dam construction in the upstream parts of a river and the growing number of water conservancy projects built along large rivers (such as freshwater withdrawal), have caused seasonal changes in downstream freshwater discharge delivery, leading to adjustments in the function of fluvial and estuarine hydrology (e.g. Lu et al., 2011; Mei et al., 2015; Dai et al., 2017). Consequently, it is important to understand the impacts of large-scale human intervention, such as flood control, navigation, salt intrusion, and freshwater withdrawal, which are relevant not only to tide-river dynamics and riparian ecology but also to sustainable water resource management in general.

River discharge generally fluctuates following a wet-dry cycle due to the seasonal variation of precipitation in the upstream river basin. For instance, the Yangtze River, the largest river in China in terms of mean discharge, which flows into the East China Sea, has a maximum river discharge during summer in July and a low value during winter in January, with a maximum discharge difference of approximately 38,000 $m^3$/s (Cai et al., 2016). Similar seasonal variations are also identified in other large rivers in

74  eastern and southern Asia, such as the Mekong River in Vietnam, Ganges River in India,

75  and Pearl River in China, under the influence of a monsoon climate. However, most

76  large rivers have been significantly dammed at the central and upper reaches in recent

77  decades, dramatically modifying stream hydrology and sediment delivery, resulting in

78  changes in hydraulics and river delta development trend at the lower reaches (e.g.

79  Räsänen et al, 2017; Rahman et al., 2018; Liu et al., 2018). Due to the fact that the

80  response of tide-river interactions to the impacts of dams are diverse and non-uniform

81  and that many more dams are to be built in the future, the impacts of the hydrodynamic

82  interactions between tidal waves and seasonal river flows from natural variations and

83  anthropogenic activities have become a common focus in international hydraulic

84  research, especially in large tidal rivers.

85

86  The Yangtze River estuary, located near the coastal area of East China Sea, is one of the

87  largest estuaries in Asia. In the mouth of the Yangtze River estuary, bifurcation occurs

88  and the characteristics of tides have been broadly investigated in previous studies (e.g.

89  Zhang et al., 2012; Lu et al., 2015; Alebregtse and Swart, 2016). However, in these

90  studies, river influences are usually neglected. In recent years, the processes of

91  nonlinear interactions between tidal wave and river flow in the Yangtze River estuary

92  have received increasing attention (e.g. Guo et al., 2015; Zhang et al., 2015a, b; Cai et

93  al., 2016; Kuang et al., 2017; Zhang et al., 2018). However, recent studies on tidal

94  properties, such as asymmetry, changes near the mouth area, and seasonal variations in

95  tidal wave propagation and fluvial effects over the entire 600 km of the tidal river, up

96    to the tidal limit of the Datong hydrological station, have been limited. In addition, the

97    operation of the Three Gorges Dam (TGD), the largest dam in the world, has

98    substantially affected the downstream river hydrology and sediment delivery. There is

99    a variety of debate regarding the potential impacts of TGD on the downstream river

100    morphology, hydrology, and ecology, since the underlying mechanism of the impact of

101    the TGD is not fully understood. Specifically, the TGD operation has altered the

102    downstream fluvial discharge and water levels on the seasonal scale, directly following

103    the reservoir seasonal impounding and release of water volume (e.g. Chen et al., 2016;

104    Guo et al., 2018). However, the impacts of seasonal freshwater regulation by the TGD

105    on the spatial-temporal tide-river dynamics in the downstream estuarine area have not

106    been systematically investigated. For example, during the dry season TGD operation

107    increased the multi-year monthly averaged river discharge at Datong station from 9520

108    $m^3 \cdot s^{-1}$ to 12896 $m^3 \cdot s^{-1}$ in January, while during wet season the regulation reduced the

109    river discharge from 49900 $m^3 \cdot s^{-1}$ to 44367 $m^3 \cdot s^{-1}$ in July during the pre- and post- TGD

110    period.

111

112    In this study, for the first time, the spatial-temporal variations in the hydrodynamic

113    processes due to the interactions of tidal flow and fluvial discharge in the Yangtze River

114    estuary caused by natural forcing and human intervention were studied, with specific

115    focus on the effect of TGD seasonal regulation. Here, we adopted a well-developed

116    analytical model proposed by Cai et al. (2014a, 2016) to investigate the spatial-temporal

117    patterns of tide-river dynamics in the entire Yangtze River estuary and quantify the

impacts of the TGD operation. In the following sections, we introduce the study site of the Yangtze River estuary. This is followed by a description of the available data and analytical model of tide-river dynamics in Section 3. Subsequently, we applied the model to the Yangtze River estuary, where the TGD has operated since 2003 (Section 4). In particular, we explored the alteration of the tide-river dynamics after the TGD closure and summarise the impacts of the TGD on the spatial-temporal patterns of tide-river dynamics. The impacts of channel geometry and river discharge alterations on tide-river dynamics as well as the implications for sustainable water resource management were then discussed in Section 5. Finally, some key findings were addressed in Section 6.

## 2. Overview of the Yangtze River estuary

The Yangtze River, flowing from west to east in central China, is one of the world's most important rivers due to its great economic and social relevance. It has a length of about 6300 km and a basin area of about 190,000 km$^2$ (Figure 1a). The Yangtze River basin is geographically divided into three parts, the upper, central, and lower sub-basins, and contains an estuary area with partitions at Yichang, Jiujiang, and Datong (DT), respectively (Figure 1a). Of concern in this study are the impacts of the Three Gorges Dam (TGD), the world's largest dam, on the spatial-temporal patterns of tide-river dynamics in the estuarine area. It is located about 45 km upstream of Yichang (Figure 1a). The TGD project began in 2003; by 2009, when full operations began, the total water storage capacity rose up to ~40 km$^3$, equivalent to 5% of the Yangtze's annual

140  discharge. Downstream the DT station, where the tidal limit is located, the Yangtze

141  River estuary extends ~630 km to the seaward end of the South Branch. Wuhu (WH),

142  Maanshan (MAS), Nanjing (NJ), Zhenjiang (ZJ), Jiangyin (JY), and Tianshenggang

143  (TSG) are the major gauging stations along the mainstream in the seaward direction

144  (Figure 1b). Under the control of the Asian monsoon climate, river discharges show

145  distinct seasonal patterns. In 1979–2012, more than 70% of freshwater was discharged

146  at DT occurred during summer (May–October).

147

148  Apart from river flows, tidal waves are also recognised as the major sources of energy

149  for hydrodynamics in the Yangtze River estuary, which is characterised by a meso-tide

150  with a tidal range of up to 4.6 m and a mean tidal range of ~2.7 m near the estuary

151  mouth. According to the observation in the Gaoqiaoju tidal gauging station (1950–

152  2012), the averaged ebb tide duration (7.5 h) is a bit longer than the averaged flood tide

153  duration (5 h), indicating an irregular semidiurnal character (Zhang et al., 2012).

154
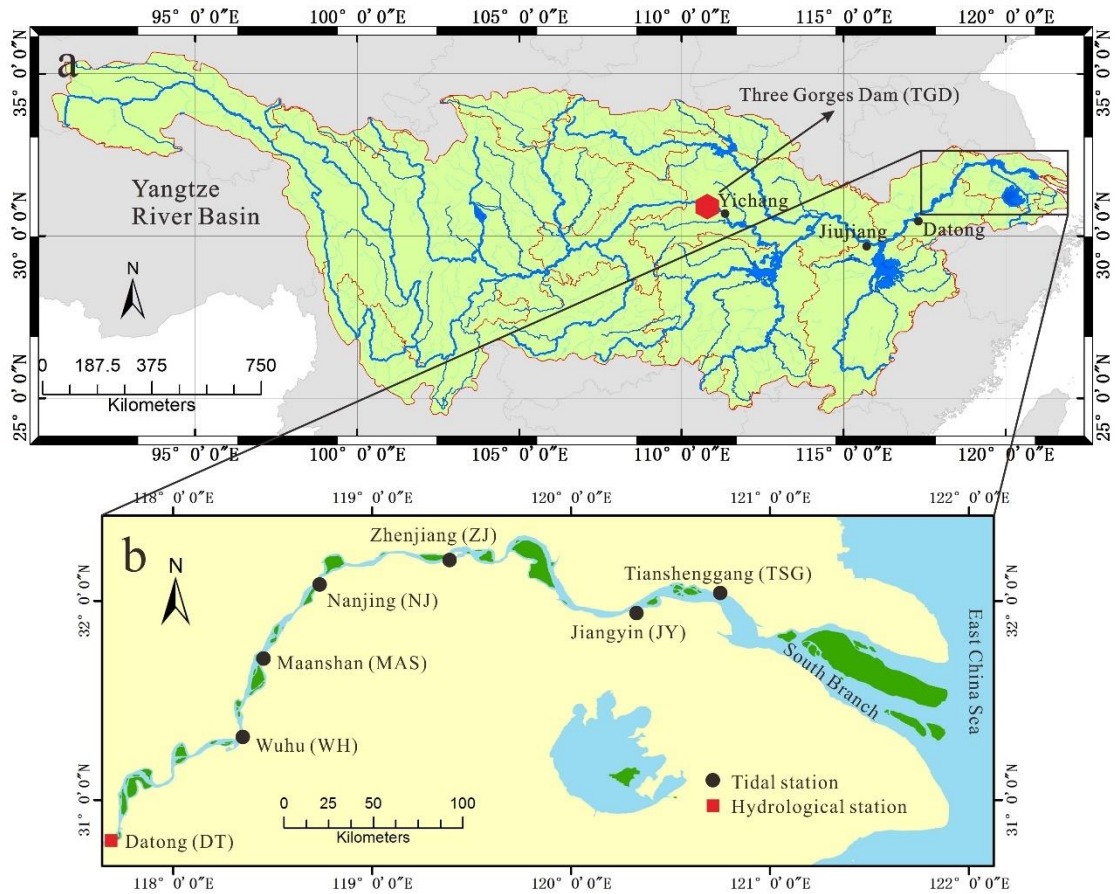
Figure 1. Maps of the Yangtze River basin (a) and Yangtze River estuary (b) with the

location of tidal gauging and hydrological stations shown with black solid circles and

red solid rectangles.

## 3. Data and Methodology

### 3.1 Source of Data

To quantitatively investigate the relationship between freshwater discharge regulation

caused by the TGD operation and the tide-river dynamics, monthly averaged

hydrological data for both pre-TGD (1979–1984) and post-TGD (2003–2014) periods

of tidal range and water level from the above-mentioned six tidal gauging stations along

the Yangtze River estuary were collected. They were published by the Yangtze

Hydrology Bureau of the People's Republic of China. The monthly averaged tidal

amplitude is determined by averaging the daily difference between high and low water

levels and dividing by two. To correctly quantify the residual water level along the

Yangtze estuary, locally measured water level at different gauging stations are corrected

to the national mean sea level of Huanghai 1985.

**3.2 Analytical model for tide-river dynamics**

**3.2.1 Basic equations**

In tidal rivers, the tidally averaged water level (i.e. residual water level) depicts a steady

gradient, which usually increases with freshwater discharge (e.g. Sassi and Hoitink,

2013). The key to deriving the dynamics of the residual water level lies in the one-

dimensional momentum equation, which can be expressed as (e.g. Savenije, 2005,

2012):

$$\frac{\partial U}{\partial t} + U\frac{\partial U}{\partial x} + g\frac{\partial Z}{\partial x} + \frac{gh}{2\rho}\frac{\partial \rho}{\partial x} + g\frac{U|U|}{K^2 h^{4/3}} = 0, \tag{1}$$

where $U$ is the cross-sectional averaged velocity, $Z$ is the free surface elevation, $h$ is the

water depth, $g$ is the acceleration due to gravity, $t$ is the time, $\rho$ is the water density, $x$ is

the longitudinal coordinate directed landward, and $K$ is the Manning-Strickler friction

coefficient. It was demonstrated that in the subtidal momentum balance, the residual

water level slope is primarily balanced by the residual friction term (Vignoli et al., 2003;

Buschman et al., 2009; Cai et al., 2014a, for a detailed derivation, readers can refer to

the Appendix A):

$$\overline{\frac{\partial Z}{\partial x}} = -\overline{\frac{U|U|}{K^2 h^{4/3}}} \tag{2}$$

where the overbars indicate the tidal average. For a single channel with the residual water level set to 0 at the estuary mouth (i.e. $\bar{Z} = 0$ at $x = 0$), the integration of Equation (2) leads to an analytical expression for the residual water level

$$\bar{Z}(x) = -\int_0^x \overline{\frac{\partial Z}{\partial x}} = -\int_0^x \overline{\frac{U|U|}{K^2 h^{4/3}}} \quad .\tag{3}$$

To derive the analytical solutions for tide-river dynamics, we assume that the longitudinal variation of cross-sectional area $\bar{A}$ and width $\bar{B}$ can be described by the following exponential functions (see also Toffolon et al., 2006; Cai et al., 2014a):

$$\bar{A} = \overline{A_r} + \left(\overline{A_0} - \overline{A_r}\right)\exp\left(-\frac{x}{a}\right),\tag{4}$$

$$\bar{B} = \overline{B_r} + \left(\overline{B_0} - \overline{B_r}\right)\exp\left(-\frac{x}{b}\right),\tag{5}$$

where $\overline{A_0}$ and $\overline{B_0}$ represent the tidally averaged cross-sectional area and width at the estuary mouth, respectively, $\overline{A_r}$ and $\overline{B_r}$ represent the asymptotic riverine cross-sectional area and width, respectively, and $a$ and $b$ are the convergence lengths of the cross-sectional area and width, respectively. The advantage of these equations for approximating the shape of the estuary is that they account not only for the exponential shape in the lower part of the tidal river but also for the approximately prismatic channel in the upstream part of the tidal river. We further assume a nearly rectangular cross-section, considering a large width to depth ratio; hence, the tidally averaged depth is given by $\bar{h} = \bar{A}/\bar{B}$ and the cross-sectional area variability can be primarily attributed to the change in depth.

**3.2.2 Analytical solution for tidal hydrodynamics**

209 It was shown by Cai et al. (2014a, b, 2016) that the tide-river dynamics is dominantly

210 controlled by four dimensionless parameters (see their definitions in Table 1). They

211 include: the dimensionless tidal amplitude $\zeta$ (representing the boundary condition in the

212 seaward side), the estuary shape number $\gamma$ (representing the cross-sectional area

213 convergence), the friction number $\chi$ (representing the bottom frictional effect), and the

214 dimensionless river discharge $\varphi$ (representing the impact of freshwater discharge). The

215 definitions of these four variables are defined in Table 1, where $\eta$ is the tidal amplitude,

216 $\upsilon$ is the velocity amplitude, $U_r$ is the river flow velocity, $\omega$ is the tidal frequency, $r_S =$

217 $B_S/\bar{B}$ is the storage width ratio between the storage width $B_S$ and the stream width $\bar{B}$

218 that accounts for the effect of storage area (i.e., tidal flats or salt marshes), and $c_0$ is the

219 classical wave celerity defined as $c_0 = \sqrt{g\bar{h}/r_S}$ .

220 Table 1. Definitions of dimensionless parameters used in the analytical model

| Local variables | Dependent variables |
|---|---|
| Dimensionless tidal amplitude | Amplification number |
| $\zeta = \eta / \bar{h}$ | $\delta = c_0 \, \mathrm{d}\eta / (\eta \omega \mathrm{d}x)$ |
| Estuary shape number | Velocity number |
| $\gamma = c_0 (\bar{A} - \bar{A}_r) / (\omega a \bar{A})$ | $\mu = \upsilon / (r_s \zeta c_0) = \upsilon \bar{h} / (r_s \eta c_0)$ |
| Friction number | Celerity number |
| $\chi = r_S g c_0 \zeta \left[1 - (4\zeta/3)^2\right]^{-1} / (\omega K^2 \bar{h}^{4/3})$ | $\lambda = c_0 / c$ |
| Dimensionless river discharge | Phase lag |
| $\varphi = U_r / \upsilon$ | $\varepsilon = \pi/2 - (\phi_z - \phi_U)$ |

221

222 In this study, we used the analytical solutions proposed by Cai et al. (2014a, b, 2016),

223 in which the solutions of the major tide-river dynamics are derived by solving a set of

224 four implicit equations for the tidal damping, the velocity amplitude, the wave celerity,

225 and the phase lag (see details in Appendix B). The major dependent parameters can be

226 described by the following four variables (see also Table 1): $\delta$ represents the

227 damping/amplification number describing the increase ($\delta > 0$), or decrease ($\delta < 0$) of

228 the tidal wave amplitude along the estuary axis, $\mu$ represents the velocity number

229 indicating the ratio of actual velocity amplitude to the frictionless value in a prismatic

230 channel, $\lambda$ represents the celerity number representing the classical wave celerity $c_0$

231 scaled by the actual wave celerity $c$, and $\varepsilon$ represents the phase lag between the high

232 water (HW) and high water slack (HWS) or between the low water (LW) and low water

233 slack (LWS). It is important to note that the phase lag (ranging between 0 and $\pi/2$) is a

234 key parameter in classifying the estuary, where $\varepsilon = 0$ suggests the tidal wave is featured

235 by a standing wave, while $\varepsilon = \pi/2$ indicates a progressive wave. For a simple harmonic

236 wave, the phase lag is defined as $\varepsilon = \pi/2 - (\phi_Z - \phi_U)$, where $\phi_Z$ and $\phi_U$ are the phases

237 of elevation and current, respectively (Savenije, et al., 2008).

238

239 **3.2.3 Analytical solution for the entire channel**

240 It is worth noting that the analytically computed tide-river dynamics $\mu$, $\delta$, $\lambda$, and $\varepsilon$ only

241 represent local hydrodynamics since they depend on local (fixed position) values of the

242 dimensionless parameters, i.e. the tidal amplitude $\zeta$, the estuary shape number $\gamma$, the

243 friction number $\chi$, and the river discharge $\varphi$ (see Table 1). To correctly reproduce the

tide-river dynamics for the entire channel, a multi-reach technique is adopted by

subdividing the entire estuary into multiple reaches to account for the longitudinal

variations of the estuarine sections (e.g. bed elevation, bottom friction). For a given

tidal damping/amplification number $\delta$ and tidal amplitude $\eta$ at the seaward boundary, it

is possible to determine the tidal amplitude at a distance $\Delta x$ (e.g. 1 km) upstream by

simple explicit integration. Hence, the analytical solution for the entire channel can be

obtained by step-wise integration in this way.

**4. Results**

**4.1 Observational analysis on the alteration of tide-river dynamics after TGD closure**

To quantify the impacts of TGD operation on the downstream tide-river dynamics, we

divided the time series into two periods, including a pre-TGD period (1979–1984,

representing the condition before the operation of the TGD) and a post-TGD period

(2003–2014, after the closure of the TGD with an operating TGD). Figure 2 shows the

changes in the observed tidal range $\Delta H$ and residual water level $\Delta \bar{Z}$ before and after

the closure of the TGD at the six gauging stations, together with the change in

freshwater discharge $\Delta Q$ observed at the DT hydrological station. Figure 2 and Table 2

clearly show that the monthly averaged river discharge in January, February, and March

substantially increased by 35.5%, 30.5%, and 16.4%, respectively, due to the

considerable release of freshwater from the TGD. On the other hand, we observe a

significant decrease in freshwater discharge in September, October, and November,

266  decreasing by 20.1%, 33.2%, and 20.8%, respectively. The reason can be primarily

267  attributed to the impounding water of the TGD during these months, especially in

268  October. During the other months, the impacts of TGD on the change in the freshwater

269  discharge are relatively small, mimicking the natural condition before the operation of

270  the TGD.

271

272  In Figure 2a we observe an increasing trend in tidal range for the post-TGD period at

273  the six gauging stations, except for the marked decrease at the ZJ station in the first half

274  of the year (i.e. January–June). On average, the maximum increase (0.20 m) in tidal

275  range occurs in October, which is mainly due to the substantial reduction of river

276  discharge caused by the TGD operation. This indicates a consistent enhancement of

277  tidal dynamics along the Yangtze estuary, except the reach near the ZJ station. The

278  exceptional case in ZJ station is likely due to the fact that ZJ station is located near the

279  position of the tidal current limit during the dry season (Guo et al., 2015; Zhang et al.,

280  2018). The shallow and narrow geometry around ZJ station impedes the tidal wave

281  propagation when river discharge increases due to the TGD operation during the dry

282  season (Chen et al., 2012), leading to a remarkably decreasing tidal range in the first

283  half of the year. For the residual water level, Figure 2b clearly shows that the change in

284  the residual water level directly follows that of the river discharge due to the stable

285  relationship between these two parameters. In particular, we see that the residual water

286  levels increased by 0.26 m, 0.30 m, and 0.16 m, respectively, in January, February, and

287  March, while they significantly decreased by 0.72 m, 1.17 m, and 0.70 m, respectively,

in September, October, and November. In addition, the decrease trend in residual water

level is more significant at upstream stations when compared with those in the

downstream areas.
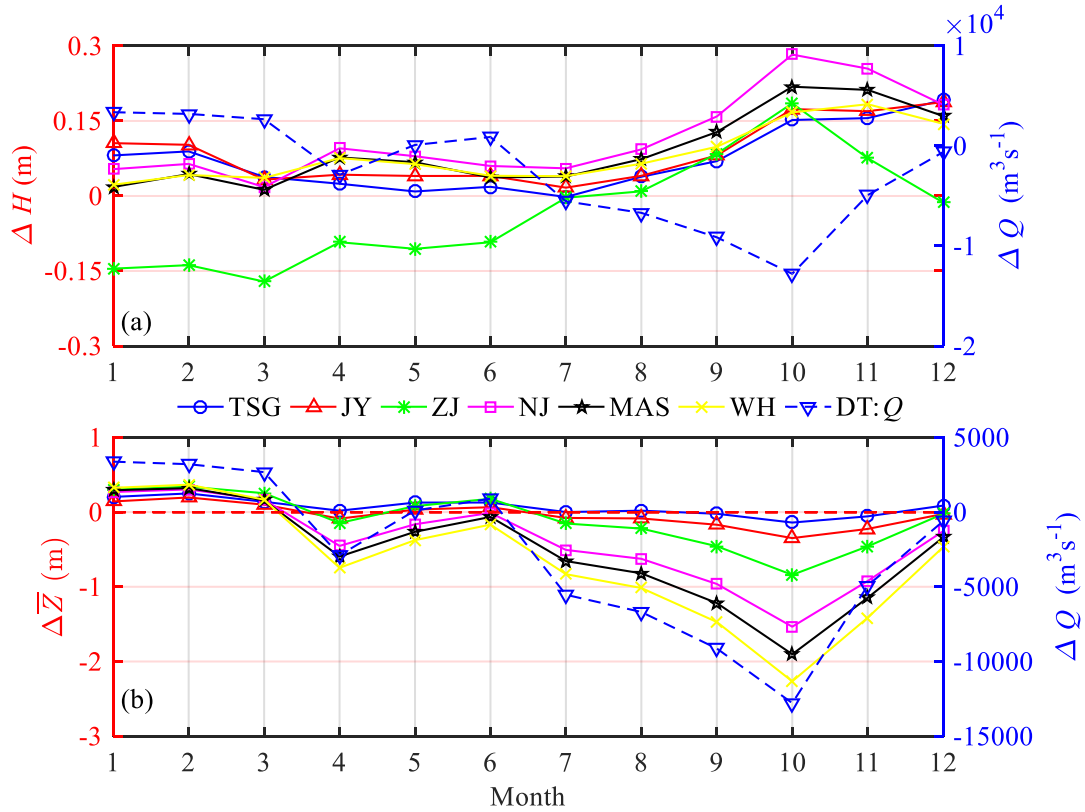
Figure 2. Changes in monthly averaged (a) tidal range $\Delta H$ and (b) residual water level

$\Delta \bar{Z}$ together with the freshwater discharge $\Delta Q$ along the Yangtze River estuary.

301    Table 2. Comparison of multi-year monthly averaged river discharge $Q$ (m$^3$·s$^{-1}$)

302    between the pre-TGD and the post-TGD periods

| Month | 1 | 2 | 3 | 4 | 5 | 6 | 7 | 8 | 9 | 10 | 11 | 12 |
|---|---|---|---|---|---|---|---|---|---|---|---|---|
| Pre-TGD | 9520 | 10527 | 16298 | 25050 | 30867 | 38283 | 49900 | 47276 | 45317 | 38467 | 23633 | 14810 |
| Post-TGD | 12896 | 13733 | 18974 | 22165 | 30971 | 39180 | 44367 | 40590 | 36187 | 25682 | 18714 | 14203 |
| Change | 3376 | 3206 | 2675 | -2885 | 105 | 896 | -5533 | -6687 | -9130 | -12784 | -4919 | -607 |

303    Since the TGD operation affects tide-river dynamics primarily through the alteration of

304    the freshwater discharge, it is worth exploring the patterns of trends in the relationship

305    between the freshwater discharge and gradients of the main tidal parameters with

306    respect to distance (i.e. the tidal damping rate and the residual water level slope). Here,

307    we estimated the tidal damping rate $\delta_H$ and the residual water level slope $S$ for a reach

308    of $\Delta x$ by using the following expressions:

$$\delta_H = \frac{1}{(H_1 + H_2)/2} \frac{H_2 - H_1}{\Delta x}, \tag{6}$$

$$S = \frac{\overline{Z_2} - \overline{Z_1}}{\Delta x}, \tag{7}$$

311    where $H_1$ and $\overline{Z_1}$ are the tidal amplitude and residual water level on the seaward side,

312    respectively, whereas $H_2$ and $\overline{Z_2}$ are the corresponding values $\Delta x$ upstream,

313    respectively. Figure 3 presents the computed tidal damping rates for different reaches

314    along the Yangtze estuary based on the observed tidal ranges at the six gauging stations.

315    It is remarkable that the tidal damping rates at the ZJ-NJ and MAS-WH reaches have

316    significantly increased during the post-TGD period, which suggests an enhancement of

317    tidal dynamics under the current freshwater discharge conditions. On the contrary, a

318    noticeable decrease in $\delta_H$ was observed at the JY-ZJ reach, which corresponds to a

319    decrease in tidal range at the ZJ station for the low river discharge conditions (from

320    January to May, see Figure 2a). At TGS-JY and NJ-MAS, no significant change in $\delta_H$

321    is observed. In Figure 4, a consistent decrease in the residual water level slope $S$ is

322    observed along the Yangtze estuary, except for the JY-ZJ reach. This means that the

323    residual friction effect becomes weaker in the post-TGD period since the residual water

324    level slope is primarily balanced by the residual friction term (Cai et al., 2014a, b, 2016).
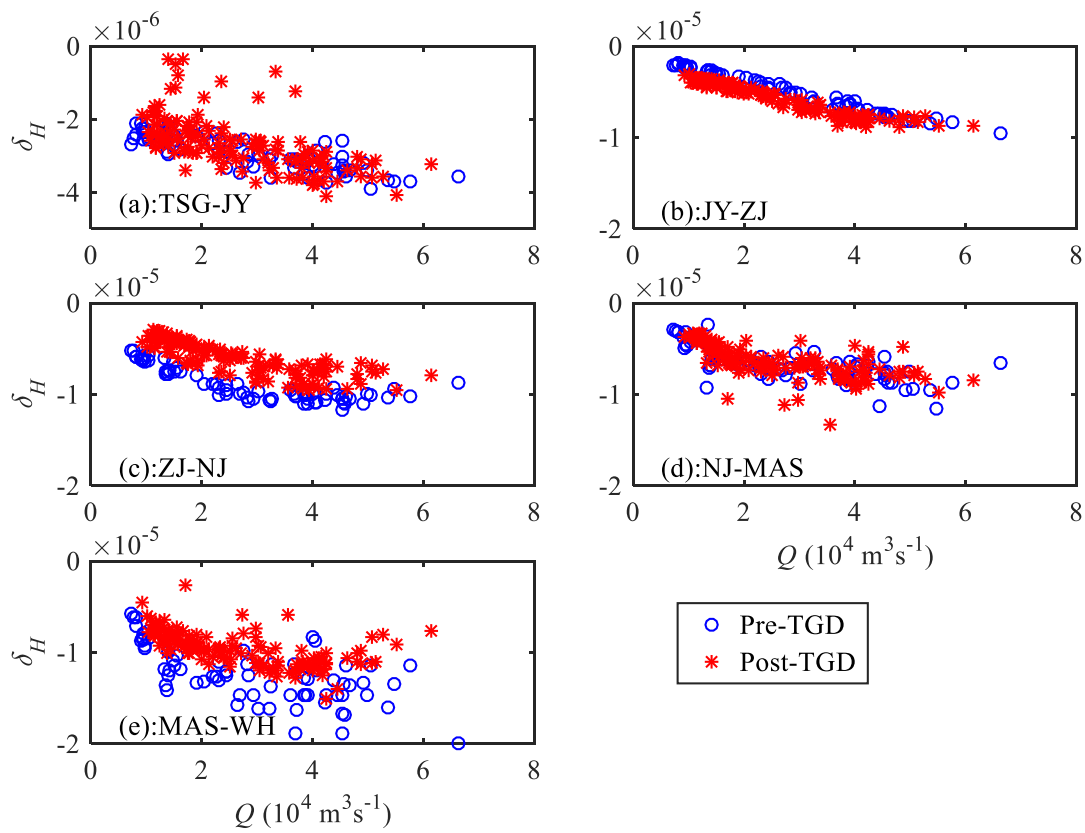
325

326    Figure 3. Changes in tidal damping rate $\delta_H$ before and after the TGD closure for

327    different reaches along the Yangtze estuary: (a) TGS-JY, (b) JY-ZJ, (c) ZJ-NJ, (d) NJ-

328    MAS, (e) MAS-WH.
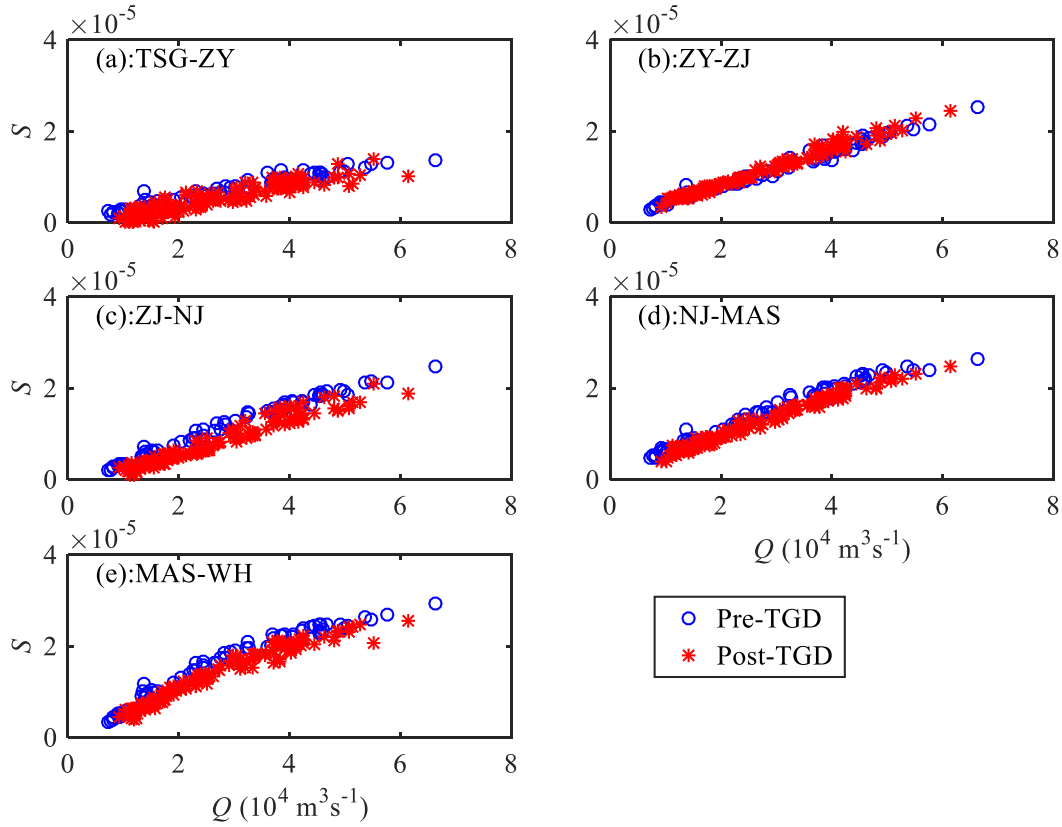
Figure 4. Changes in residual water level slope $S$ before and after the TGD closure for different reaches along the Yangtze estuary: (a) TGS-JY, (b) JY-ZJ, (c) ZJ-NJ, (d) NJ-MAS, (e) MAS-WH.

## 4.2 Performance of the analytical model reproducing the tide-river dynamics

The analytical model presented in Section 3.2 was subsequently applied to the Yangtze River estuary, with the seaward boundary using the tidal amplitude imposed at the TSG station and the landward boundary using the river discharge imposed at the DT station. The computation length of the estuary is 470 km, covering the entire estuary from TSG to DT. The adopted geometric characteristics (including the tidally averaged cross-sectional area, width, and depth) are the same for both pre- and post-TGD periods, which were extracted from a digital elevation model (DEM) using Yangtze River

342     estuary navigation charts surveyed in 2007. The geometric characteristics, calibrated

343     by fitting the observed values using Equations (4) and (5), are presented in Table 3,

344     where a relatively large cross-sectional area convergence length ($a = 151$ km) is evident,

345     with a relatively small width ($b = 44$ km), indicating a fast transition from a funnel-

346     shaped reach to a prismatic reach in terms of width. It is worth noting that the Yangtze

347     River estuary is characterised by a typical semidiurnal character; thus, a typical $M_2$ tidal

348     period (i.e. 12.42 h) was adopted in the analytical model. For the sake of simplification,

349     we assume that the storage width ratio $r_S = 1$. Hence, the only calibrated parameter is

350     the Manning-Strickler friction coefficient $K$. Here, we used two values for $K$: $K = 80$

351     $m^{1/3} \cdot s^{-1}$ in the tide-dominated region ($x = 0$–32 km), and a smaller value of $K = 55$

352     $m^{1/3} \cdot s^{-1}$ in the river-dominated region ($x = 52$–450 km). In addition, to avoid sharp jump

353     in the analytically computed parameters due to the adoption of different friction

354     coefficients, we adopted a friction coefficient of $K=80$-55 $m^{1/3}s^{-1}$ (indicating a linear

355     reduction of the friction coefficient) over the transitional reach ($x=32$-52 km). The

356     analytically computed results were compared with the observed tidal amplitudes and

357     the residual water levels at five gauging stations along the Yangtze estuary (Figure 5).

358     It can be seen that the overall correspondence between analytical results and

359     observations is good, with high coefficients of determination ($R^2 > 0.95$), which

360     suggests the usefulness of the present analytical model for reproducing the tide-river

361     dynamics, given the gross features of flow characteristics and estuarine geometry.

362

363

Table 3. Characteristics of geometric parameters in the Yangtze River estuary

| Characteristics | River | Mouth | Convergence length $a/b$ (km) |
|---|---|---|---|
| Cross-sectional area $\bar{A}$ (m$^2$) | 12,135 | 51,776 | 151 |
| Width $\bar{B}$ (m) | 2005 | 6735 | 44 |

365

366
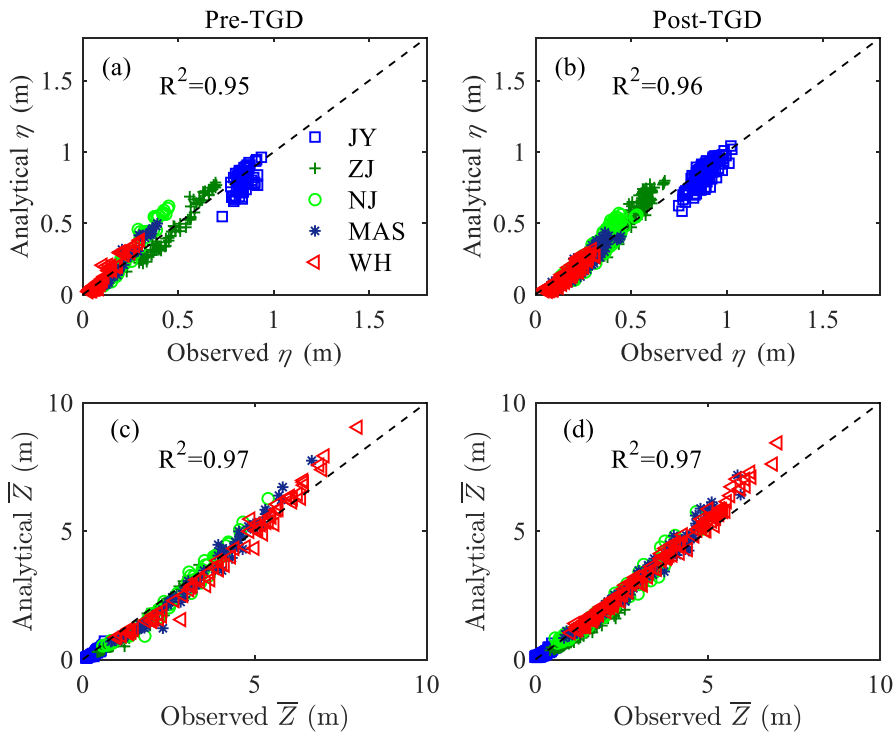
Figure 5. Comparison of monthly averaged values for (a, b) analytically computed tidal

amplitude $\eta$ and (c, d) residual water level $\bar{Z}$ against the observations in the Yangtze

River estuary for the pre-TGD period (1979–1984) and post-TGD period (2003–2014).

370

**4.3 Impacts of TGD operation on spatial-temporal patterns of tide-river dynamics**

With the significant seasonal discharge variations resulting from the TGD regulation,

an understanding of the seasonal impacts on tide-river dynamics along the estuary has

374 become increasingly important. In Figures 6 and 7, we see how the TGD operation

375 impacts the longitudinal variation of the main tidal dynamics in terms of the four

376 dependent parameters $\delta$, $\lambda$, $\mu$, and $\varepsilon$ for different seasons. The most considerable changes

377 in the major tide-river dynamics occurred in both autumn and winter seasons, which

378 correspond to the substantial reduction in freshwater discharge in the wet-to-dry

379 transition period (i.e. autumn) and slightly increased freshwater discharge in the dry

380 season (i.e. winter) due to the TGD operation since 2003 (see Table 2). On the other

381 hand, the impacts of the TGD operation on the tide-river dynamics during the spring

382 and summer are relatively minor due to the negligible change in the freshwater

383 discharge. However, we do notice that the TGD had exerted slight influence on tide-

384 river dynamics in the downstream reaches ($x < 250$ km) during the summer, with the

385 maximum freshwater discharge occurring within a year. In addition, it appears that there

386 exists a critical position corresponding to the maximum tidal damping (or minimum

387 value of $\delta$) upstream in which the tidal damping becomes weak. This phenomenon

388 occurs particularly in the spring, summer, and autumn. The underlying mechanism is

389 elaborated in the discussion section.

390

391 Figures 6a, c, e, g show the comparison of the analytically computed tidal damping

392 number $\delta$ before and after the closure of the TGD, in which we clearly observe that the

393 longitudinal tidal damping effect was considerably weakened in autumn, while it was

394 slightly enhanced in winter after the TGD closure. This was expected since freshwater

395 discharges tend to dampen the tidal wave primarily through the enhancement of the

396     friction term (Horrevoets et al., 2004; Cai et al., 2014a, b, 2016). Figures 6b, d, g, i

397     show a similar picture for the wave celerity number $\lambda$, which is positively correlated to

398     the tidal damping number $\delta$, according to the celerity equation (11) in Appendix B.

399     Figure 7 shows the longitudinal computation of the velocity number $\mu$ and the phase

400     lag $\varepsilon$ for both periods. The impacts of the TGD operation on the velocity scale and phase

401     lag are similar to the tidal damping, i.e. the larger the freshwater discharge, the smaller

402     the velocity number and the phase lag. In Figures 6 and 7, there exist switches of the

403     analytically computed parameters at both ends of the transitional reach ($x$=32-52 km)

404     owing to the change in friction coefficient adopted in the analytical model.

405

406     Overall, in the seaward reach of the estuary, the effect of freshwater discharge alteration

407     by the TGD operation on the major tide-river dynamics (i.e. $\delta$, $\lambda$, $\mu$, and $\varepsilon$) was less

408     significant because of the small ratio of freshwater discharge to tidal discharge. On the

409     other hand, in the upstream reach of the estuary, the changes in the four dependent

410     parameters are also small due to the substantial tidal attenuation as a result of the long-

411     distance propagation from the estuary mouth. Therefore, the pattern of seasonal

412     variation due to the TGD operation is relatively small at both ends of the estuary,

413     whereas the largest variation usually occurs in the middle reach of the estuary. This

414     finding was supported by the results of harmonic analysis using the numerical results

415     (Zhang et al., 2018). Similar phenomena have also been identified in other large fluvial

416     meso-tide estuaries, such as the Mekong River estuary and Amazon River estuary,

417     where dam operation altered the seasonal patterns of tide-river dynamics (Kosuth et al.,

418    2009; Hecht et al., 2018).

419
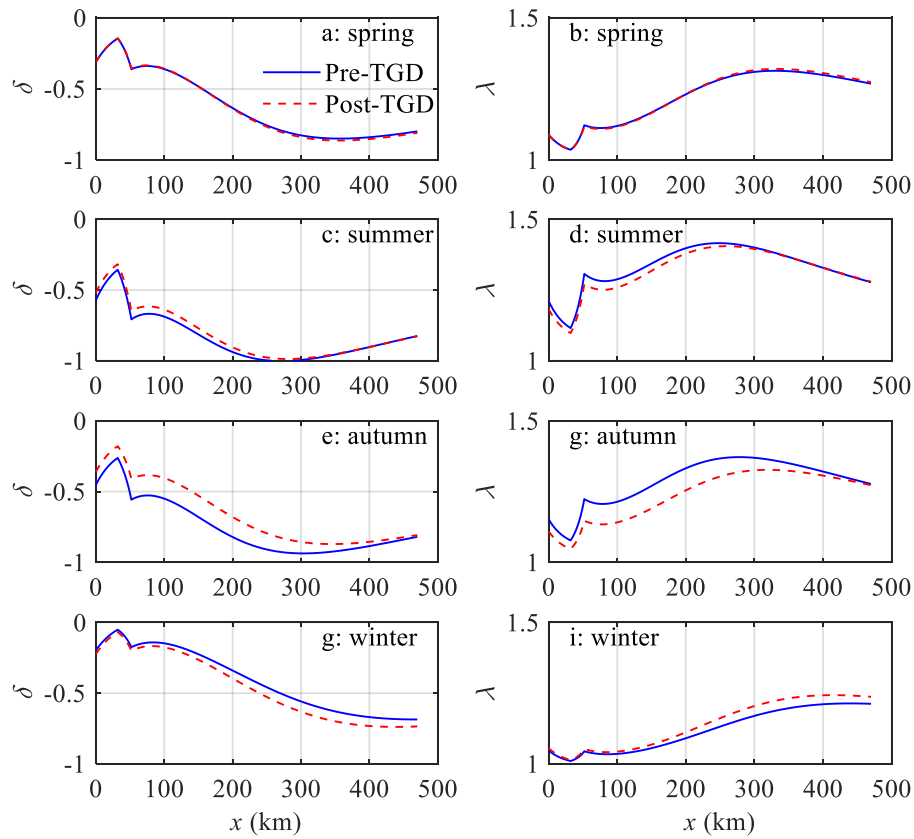
420    Figure 6. Longitudinal variability of simulated tidal damping number $\delta$ (a, c, e, g) and

421    celerity number $\lambda$ (b, d, g, i) along the Yangtze estuary in different seasons (spring: a,

422    b; summer: c, d; autumn: e, g; winter: g, i) for both the pre-TGD and the post-TGD

423    periods.

424
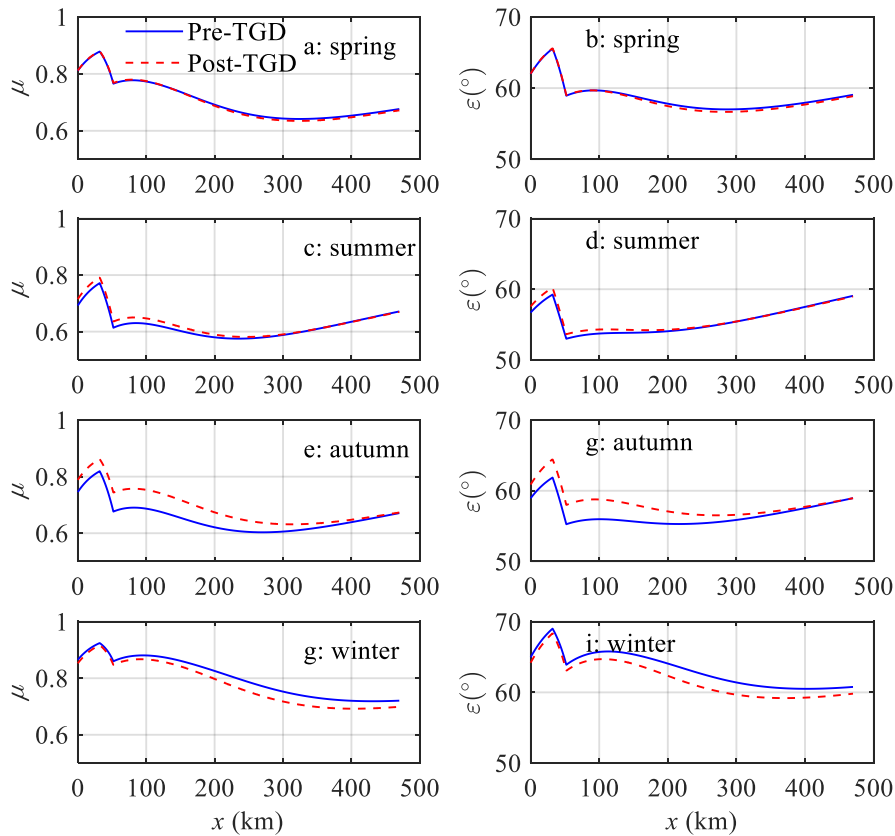
Figure 7. Longitudinal variability of simulated velocity number $\mu$ (a, c, e, g) and phase

lag $\varepsilon$ (b, d, g, i) along the Yangtze estuary in different seasons (spring: a, b; summer: c,

d; autumn: e, g; winter: g, i) for both the pre-TGD and the post-TGD periods.

428

## 5. Discussion

### 5.1 The impact of channel geometry alteration on tide-river dynamics

Dam operations, which dramatically modified downstream flow and sediment regimes,

are becoming an increasingly important factor controlling the morphological evolution.

Previous studies show that, as a result of the trapping of sediments by the TGD,

considerable erosion occurred in the first several hundred km downstream of the TGD,

considerably coarsening the bedload (Yang et al., 2014). In particular, the river bed

436    immediately downstream was eroded at a rate of 65 Mt/yr in 2001–2002 (Yang et al.,

437    2014). It was shown by Lyu et al. (2018) that due to a dramatic reduction in the sediment

438    discharge following the construction of the TGD, a significant change in size, geometry,

439    and spatial distribution of pool-riffles occurred downstream; however, this adjustment

440    was limited to the reaches close to the TGD. It should be noted that the bathymetry

441    adopted in the analytical model is restricted to the estuarine area in 2007, which is only

442    4 years after the TGD closure in 2003, and it is before the full operation of the TGD

443    began in 2009. In addition, the TGD is around 1600 km away from the estuary mouth,

444    and its influence on the estuarine morphology normally has a lag effect of at least 4–5

445    years, as discussed by Wang et al. (2008). Hence, the adopted geometry has been only

446    partly altered after the TGD closure. The morphological change of Yangtze Estuary can

447    be even more profound in recent years due to the continuous and accumulated impact

448    from the TGD. Further adjustment of morphological change due to the sedimentation

449    in the TGD could exert a considerable impact on the tide-river dynamics in the estuarine

450    region (e.g., Du et al., 2018; Shaikh et al., 2018). Further study on the impact of

451    morphological adjustment on the tide-river dynamics is required in the future.

452

453    **5.2 The impact of freshwater discharge alteration on tide-river dynamics**

454    The water conservancy of the TGD has multiple purposes, in which the seasonal

455    discharge regulation and their impact on the ecosystem are well documented (e.g. Mei

456    et al., 2015a, b; Chen et al., 2016; Guo et al., 2018). However, the actual influence of

457    discharge regulation on the river-tide dynamics in the estuarine area is not fully

458    understood. With the analytical reproduction of tide-river dynamics for pre- and post-

459    TGD periods, it is possible to quantify the extent of the changes in the major tidal

460    dynamics, including the estuary shape number $\gamma$ and friction number $\chi$ (Figure 8), and

461    the residual water level slope $S$ and water depth $h$ (Figure 9) along the Yangtze River

462    estuary. In general, during the transition from the wet season (summer–autumn) to the

463    dry season (winter–spring), the water level and corresponding fluvial discharge

464    downstream from the TGD is first raised by the impounding water and then reduced by

465    the release of water, which would substantially change the tide-river dynamics in the

466    downstream estuarine area, with the maximum variation occurring in autumn and the

467    minimum variation occurring in spring.

468
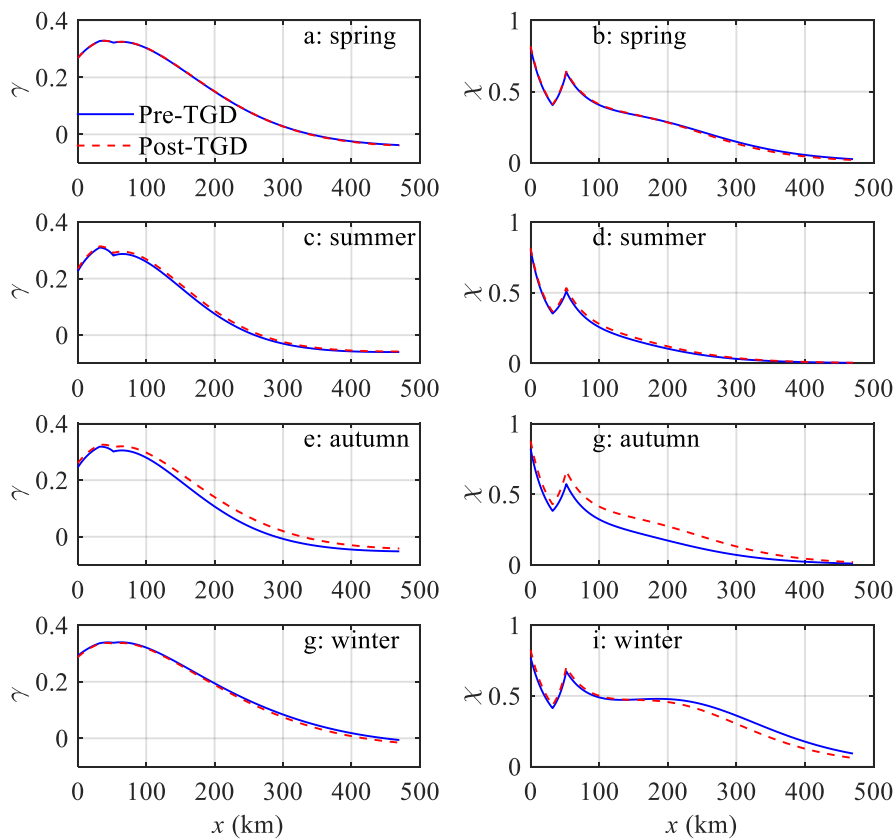
469

470     Figure 8. Longitudinal variability of simulated estuary shape number $\gamma$ (a, c, e, g) and

471     friction number $\chi$ (b, d, g, i) along the Yangtze estuary in different seasons (spring: a, b;

472     summer: c, d; autumn: e, g; winter: g, i) for both the pre-TGD and the post-TGD periods.
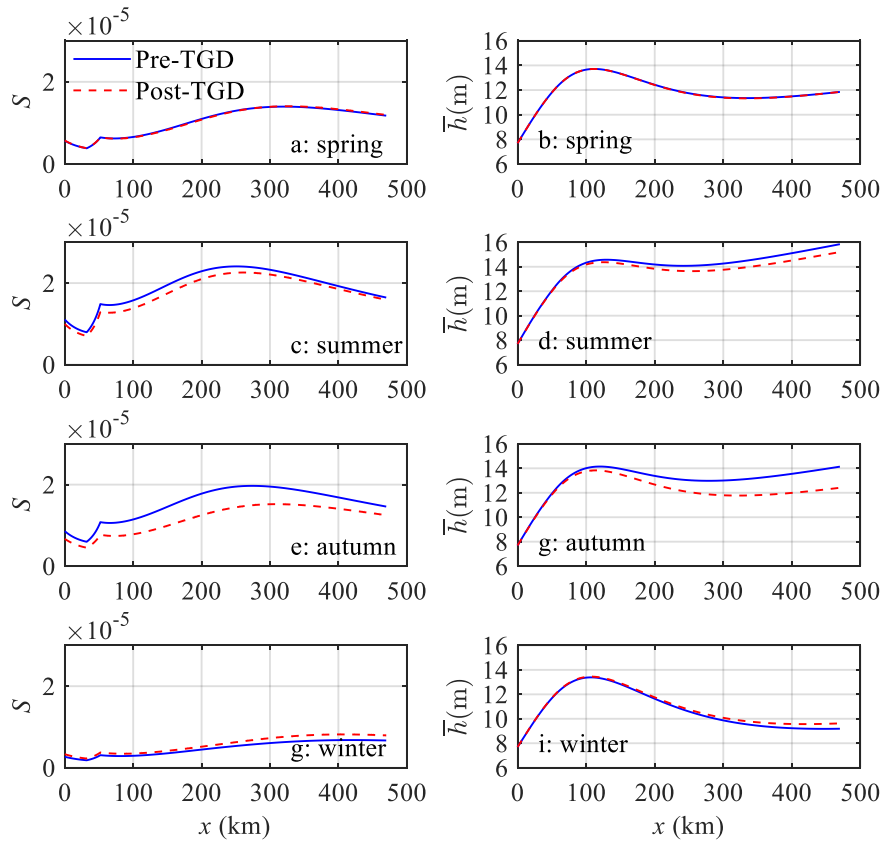
473

474     Figure 9. Longitudinal variability of simulated residual water level slope $S$ (a, c, e, g)

475     and water depth $h$ (b, d, g, i) along the Yangtze estuary in different seasons (spring: a,

476     b; summer: c, d; autumn: e, g; winter: g, i) for both the pre-TGD and the post-TGD

477     periods.

478

479     Figures 8 and 9 show that during the wet season (summer–autumn), the estuary shape

480     number $\gamma$ and friction number $\chi$ experience a general increase, while a decrease in the

481     residual water level slope $S$ and water depth $\bar{h}$ can be identified in the post-TGD

period due to the reduction in freshwater discharge. However, the changes in these major dynamics vary significantly along the channel. Near the estuary mouth, where tidal influence overwhelms the influence from freshwater discharge, the difference is relatively small, as the magnitude of the freshwater discharge is small when compared with that of the tidal discharge. Meanwhile at the upstream reach of the estuary, where the riverine influence dominates that of the tide, the difference is also small due to the attenuation of the tidal wave propagation over a long distance. Consequently, the most significant changes in major tide-river dynamics occurred in the middle reach of the Yangtze River estuary due to the discharge regulation of the TGD during the wet season. By contrast, during the dry season (winter–spring), especially in winter, the opposite trend was observed, indicating a slight increase in $\gamma$ and $\chi$, and a slight decrease in $S$ and $\bar{h}$ due to the additional release of discharge from the TGD. In addition, we also observed that the changes in tide-river dynamics caused by the TGD operation were much stronger upstream than in the lower stream.

### 5.3 Implications for water resource management

The construction of the TGD is the largest hydro-development project ever performed in the world, having multiple influences on downstream water resource management, including navigation, flood control, tidal limit variation, and salt intrusion.

### 5.3.1 Implications for navigation

The navigation condition is mainly controlled by both high water and low water levels.

504    Figure 10 shows the estimation of the cumulative distribution function (cdf) for both

505    the high-water level (Figure 10a) and the low-water level (Figure 10b) at the six

506    gauging stations along the Yangtze River estuary for both the pre- and post-TGD

507    periods. The results indicate that navigation conditions during the non-flood season are

508    generally improved, because both percentages of high-water and low-water levels are

509    increased due to the additional freshwater discharge released from the TGD. On the

510    other hand, during the flood season, the reduction in the freshwater discharge by TGD

511    impounding tends to exert a negative impact on navigation. However, the reduced

512    freshwater discharges in the late summer and autumn are not of sufficient magnitude to

513    cause any navigation problems. This is due to the fact that the mean water levels during

514    the flood season are relatively high; hence, the regulating flow quantity and regulating

515    capacity are relatively small (e.g. Chen et al., 2016). In general, due to the staggered

516    regulation in freshwater discharge, seasonally, the actual navigation condition is

517    improved due to the significant increase in the percentage of low water levels.
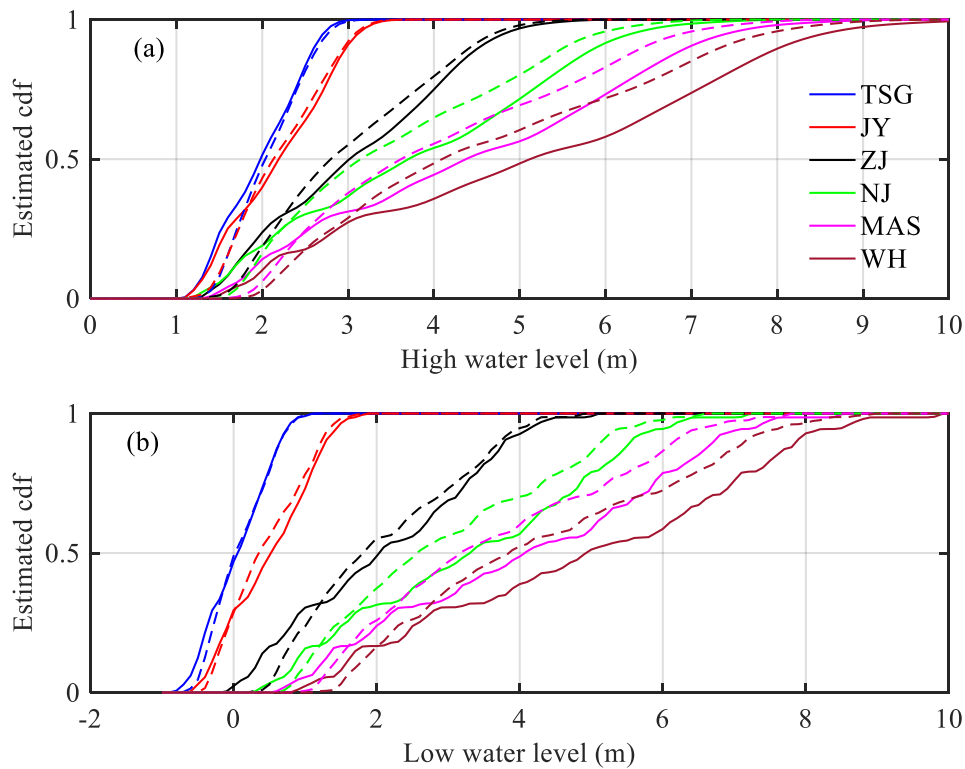
Figure 10. Cumulative distribution function (cdf) estimated by using the kernel smoothing function (a) for high water level and (b) low water level at six gauging stations along the Yangtze estuary. The solid lines represent the pre-TGD period, while the dashed lines represent the post-TGD period.

### 5.3.2 Implications for flood control

Flood control is one of the most important functions of building dams and reservoirs in large rivers. Before the construction of the TGD, the Yangtze River basin suffered from frequent and disastrous flood threats. For instance, the floods of 1998 in the Yangtze River were reported to have killed 3656 people, destroyed 5.7 million homes, and damaged seven million more. Many studies have examined the flood control capacity of the TGD over the past two decades (Zhao et al., 2013; Chen et al., 2014). In particular, the capability of the TGD flood control is influenced by multiple factors (e.g. Huang et

al., 2018), particularly in the estuarine area, which is strongly influenced by tides from the ocean. During the flood season, the reduced freshwater discharge by TGD impounding benefits the flood control by reducing the peak flood discharge. However, as the tidal influence is enhanced, both the percentages of high water and low water levels for the post-TGD period are considerably increased, as shown in Figure 10, indicating a decreased flood control capability. For instance, at the WH gauging station located in the upstream part of the Yangtze River estuary, the 8-m high-water level increased by approximately 10% after the TGD closure during the wet season. The corresponding flood prevention standard, therefore, is reduced due to the increased high-water level (see also Nakayama and Shankman, 2013).

### 5.3.3   Implications for tidal limit

It is important to detect the position of the tidal limit (corresponding with the position where the tidal amplitude to depth ratio is less than a certain threshold, e.g. $\frac{\eta}{h} < 0.02$), which is the farthest point upstream where a river is affected by tidal fluctuations, since it is essential for surveying, navigation, and fisheries management, in general (e.g. Shi et al., 2018). Subsequently, we are able to define the tide-influenced length as the distance upstream from the estuary mouth to the tidal limit. Generally, the tidal limit fluctuates with the changes in the seasonal freshwater discharges. Field measurements have demonstrated that tidal limit can reach as far as the NJ station and further upstream during the dry season, while during the wet season, it is pushed down to the ZJ station and may be pushed further downward to the JY station under spate conditions. Figure 11 shows the analytically computed tidal limit position for both the pre- and post-TGD

periods. It can be observed that the tidal limit moved downstream by about 45 km and
39 km in January and February under the impact of the additional release of discharge
from TGD during the dry season. During the transition from dry to wet seasons
(January–May), the total freshwater discharge from TGD increases, and we identify
further downstream movement of the tidal limit, although to a smaller extent. The
reverse of the post-TGD tidal limit in April is due to the decrease in the freshwater
discharge compared with the pre-TGD tidal limit (see Table 2). The TGD storage period
begins in June, and the tidal limit moved upstream by a large amount compared with
the pre-TGD period. The largest change occurred during October when the tidal limit
moved from 175 km pre-TGD to 250 km post-TGD due to the substantial increase in
freshwater discharge (see Table 2).
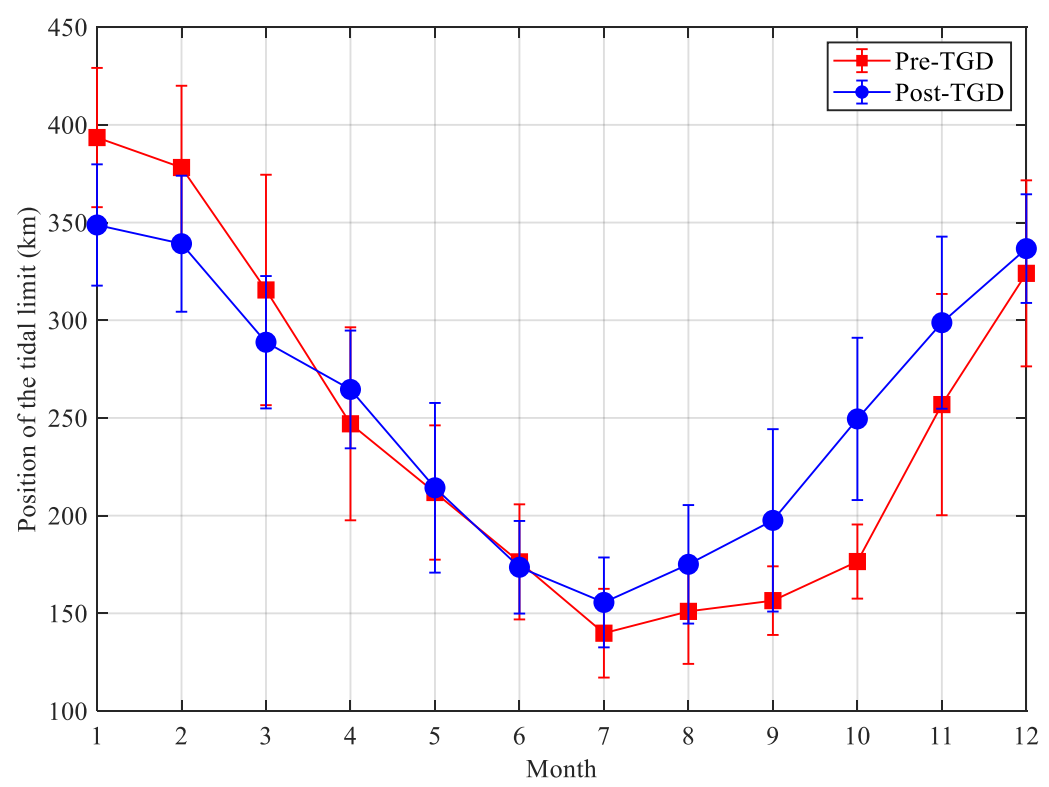
568    Figure 11. Temporal variation of the position of the tidal limit relative to the TSG station

569    for both the pre-TGD and the post-TGD periods. The vertical error bar at each data

570    point indicates the standard deviation of the analytically computed time series.

571

### 5.3.4   Implications for salt intrusion

573    The operation of the TGD changed the location of tidal limit, which, in turn, directly

574    influences the intensity of saltwater intrusion, especially during the dry season, when

575    the freshwater discharge is low and saltwater intrusion is important (e.g. Cai et al.,

576    2015). The analysis of tide-river dynamics shows that the tidal dynamics are

577    considerably enhanced during the autumn due to the substantial decline in freshwater

578    discharged into the estuary, which may lead to enhanced saltwater intrusion. However,

579    with supplemented discharge after the TGD during the winter, saltwater intrusion tends

580    to be significantly suppressed, and the isohalines are pushed seaward by additional river

581    discharges (e.g. An et al., 2009; Qiu and Zhu, 2013). In contrast, during the wet season,

582    the TGD operation slightly extended the timing of saltwater intrusion and increased its

583    intensity by impounding freshwater. Since the total river discharge rate during the wet

584    season is the largest during the year, the influence of saltwater on freshwater reservoirs

585    along the coastal area is limited. Therefore, the operation of TGD is overall favourable

586    for reducing the burden of freshwater supplement in the tidally influenced estuarine

587    areas. However, to quantify the potential impacts of TGD's operation on salt intrusion

588    and related aquatic ecosystem health in general, it is required to couple the

589    hydrodynamic model to the ecological or salt intrusion model (e.g., Qiu and Zhu, 2013;

590    Cai et al., 2015).

591

**6.  Conclusions**

An analytical approach was used to examine the potential impacts of TGD operation

on the spatial-temporal patterns of tide-river dynamics along the Yangtze River estuary.

It was shown that the freshwater regulation caused by the TGD, on a seasonal scale,

exerts significant impacts on the tide-river dynamics, with the maximum influence

occurring in autumn and winter. This generally corresponds to a dramatic decrease in

freshwater discharge during the wet-to-dry transition period and a slight increase in

discharge during the dry season. The analytical results indicate that the discharge

regulation by the TGD drives the alterations in the tide-river dynamics instead of the

geometric change. In particular, the change in the freshwater discharge changes the

estuary shape number (representing the geometric effect), the residual water level slope

(representing the effective frictional effect) and, hence, the tide-river dynamics. This

study, using the Yangtze River estuary as an example, provides an effective yet simple

method to quantify the seasonal regulation in freshwater discharge by large reservoirs

or dams on hydrodynamics in estuaries. The results obtained from this study will,

hopefully, shed new light on aspects of water resource management, such as navigation,

flood control, and salt intrusion.

609

**Data availability.** Data and results are available from the authors upon request.

**Author contributions.** All authors contributed to the design and development of the

work. The experiments were originally carried out by Huayang Cai. Xianyi Zhang and

Leicheng Guo carried out the data analysis. Min Zhang built the model and wrote the

paper. Feng Liu and Qingshu Yang reviewed the paper.

**Competing interests.** The authors declare that they have no conflict of interest.

**Acknowledgments.** We acknowledge the financial support from the National Key R&D of China (Grant No. 2016YFC0402600), from the Open Research Fund of State Key Laboratory of Estuarine and Coastal Research (Grant No. SKLEC-KF201809), from the National Natural Science Foundation of China (Grant No. 51709287 and 41701001), and from the Guangdong Provincial Natural Science Foundation of China (Grant No. 2017A030310321).

**References**

An, Q., Wu., Y., and Taylor, S.: Influence of the Three Gorges Project on saltwater intrusion in the Yangtze River Estuary, Environ. Geol., 56, 1679-1686, https://doi.org/10.1007/s00254-008-1266-4, 2009.

Alebregtse, N. C., and de Swart, H. E.: Effect of river discharge and geometry on tides and net water transport in an estuarine network, an idealized model applied to the Yangtze estuary, Cont. Shelf. Res., 123, 29-49, https://doi.org/10.1016/j.csr.2016.03.028, 2016.

Buschman, F. A., Hoitink, A. J. F., van der Vegt, M., and Hoekstra, P.: Subtidal water level variation controlled by river flow and tides, Water Resour. Res., 45(10), W10420, https://doi.org/10.1029/2009WR008167, 2009.

Cai, H., Savenije, H. H. G., and Toffolon, M.: Linking the river to the estuary, influence

of river discharge on tidal damping, Hydrol. Earth Syst. Sci., 18(1), 287-304, https://doi.org/10.5194/hess-18-287-2014, 2014a.

Cai, H., Savenije, H. H. G., and Jiang, C.: Analytical approach for predicting fresh water discharge in an estuary based on tidal water level observations, Hydrol. Earth Syst. Sci., 18(10), 4153-4168, https://doi.org/10.5194/hess-18-4153-2014, 2014b.

Cai, H., Savenije, H.H.G., Zuo, S., Jiang, C., and Chua, V.: A predictive model for salt intrusion in estuaries applied to the Yangtze estuary, J. Hydrol., 529, 1336-1349, https://doi.org/10.1016/j.jhydrol.2015.08.050, 2015.

Cai, H., Savenije, H. H. G., Jiang, C. Zhao L., Yang Q.: Analytical approach for determining the mean water level profile in an estuary with substantial fresh water discharge, Hydrol. Earth Syst. Sci., 20, 1-19, https://doi.org/10.5194/hess-20-1-2016, 2016.

Chen, J., Finlayson, B.L., Wei, T., Sun, Q., Webber, M., Li, M., and Chen, Z.: Changes in monthly flows in the Yangtze River, China-With special reference to the Three Gorges Dam, J. Hydrol., 536, 293-301, https://doi.org/10.1016/j.jhydrol. 2016.03.008, 2016.

Chen, J., Wang, Z., Li, M., Wei, T. and Chen, Z.: Bedform characteristics during falling flood stage and morphodynamic interpretation of the middle–lower Changjiang (Yangtze) River channel, China, Geomorphology, 147, 18-26, https://10.1016/j.geomorph.2011.06.042, 2012.

Chen, J., Zhong, P.A., Zhao, Y.F.: Research on a layered coupling optimal operation model of the Three Gorges and Gezhouba cascade hydropower stations, Energy

Convers. Manage. 86 (5), 756–763, https://doi.org/10.1016/j.enconman.2014.06.043, 2014.

Dai, M., Wang, J., Zhang, M., and Chen, X.: Impact of the Three Gorges Project operation on the water exchange between Dongting Lake and the Yangtze River, Int. J. Sediment Res., 32, 506-514, https://doi.org/10.1016/j.ijsrc.2017.02.006, 2017.

Dronkers, J. J.: Tidal Computations in River and Coastal Waters, Elsevier, New York, USA, https://doi.org/10.1126/science.146.3642.390, 1964.

Du, J., Shen, J., Zhang, Y.J., Ye, F., Liu, Z., Wang, Z., Wang, Y.P., Yu, X., Sisson, M., Wang, H.V.: Tidal Response to Sea-Level Rise in Different Types of Estuaries: The Importance of Length, Bathymetry, and Geometry, Geophys Res Lett., 45(1), 227-235, https://doi.org/10.1002/2017GL075963, 2018.

Guo, L., van der Wegen, M., Jay, D.A., Matte, P., Wang, Z.B., Roelvink, D.J.A., He, Q.: River-tide dynamics, Exploration of nonstationary and nonlinear tidal behavior in the Yangtze River estuary, J. Geophys. Res., 120(5), 3499-3521, https://doi.org/10.1002/2014JC010491, 2015.

Guo, L., Su, N., Zhu, C., and He, Q.: How have the river discharges and sediment loads changed in the Changjiang River basin downstream of the Three Gorges Dam? J. Hydrol., 560, 259-274, https://doi.org/10.1016/j.jhydrol.2018.03.035, 2018.

Guo, L., van der Wegen, M., Jay, D.A., Matte, P., Wang, Z.B., Roelvink, D., and He, Q.: River-tide dynamics: Exploration of nonstationary and nonlinear tidal behavior in the Yangtze River Estuary, J. Geophys. Res., 120(5), 3499-3521, https://10.1002/2014JC010491, 2015.

678  Hoitink, A. J. F., and Jay, D. A.: Tidal river dynamics: implications for deltas, Rev.

679  Geophys., 54, 240-272, https://doi.org/10.1002/2015RG000507, 2016.

680  Hoitink, A. J. F.,Wang, Z. B., Vermeulen, B., Huismans, Y., and Kastner, K.: Tidal

681  controls on river delta morphology, Nat. Geosci., https://doi.org/10, 10.1038/ngeo3000,

682  2017.

683  Horrevoets, A. C., Savenije, H. H. G., Schuurman, J. N., and Graas, S.: The influence

684  of river discharge on tidal damping in alluvial estuaries, J. Hydrol., 294, 213-228,

685  https://doi.org/10.1016/j.jhydrol.2004.02.012, 2004.

686  Hecht, J.S., Lacombe, G., Arias, M.E., Duc Dang, T. and Piman, T.: Hydropower dams

687  of the Mekong River basin, a review of their hydrological impacts, J. Hydrol., 45(10):

688  W10420, https://doi.org/10.1016/j.jhydrol.2018.10.045, 2018.

689  Huang, K., Ye, L., Chen, L., Wang, Q., Dai, L., Zhou, J., Singh, V. P., Huang, M., and

690  Zhang, J.: Risk analysis of flood control reservoir operation considering multiple

691  uncertainties, J. Hydrol., 565, 672-684, https://doi.org/10.1016/j.jhydrol.2018.08.040,

692  2018.

693  Kuang, C., Chen, W., Gu, J., Su, T. C., Song, H., Ma, Y., and Dong, Z.: River discharge

694  contribution to sea-level rise in the Yangtze River Estuary, China, Cont. Shelf. Res.,

695  134, 63-75, https://doi.org/10.1016/j.csr.2017.01.004, 2017.

696  Kosuth, P., Callède, J., Laraque, A., Filizola, N., Guyot, J.L., Seyler, P., Fritsch, J.M.,

697  and Guimarães, V.: Sea-tide effects on flows in the lower reaches of the Amazon River,

698  Hydrol. Process., 23(22), 3141-3150, https://doi.org/10.1002/hyp.7387, 2009.

699  Liu, F., Hu, S., Guo, X., Cai, H., Yang, Q.: Recent changes in the sediment regime of

the Pearl River (South China), Causes and implications for the Pearl River Delta, Hydrol. Process., 32(12): 1771-1785, https://doi.org/10.1002/hyp.11513, 2018.

Lu, S., Tong, C., Lee, D.Y., Zheng, J., Shen, J., Zhang, W., and Yan, Y.: Propagation of tidal waves up in Yangtze Estuary during the dry season, J. Geophys. Res., 120(9), 6445-6473, https://doi.org/10.1002/2014JC010414, 2015.

Lu, X.X., Yang, X., and Li, S.: Dam not sole cause of Chinese drought, Nature 475(7355), 174, https://doi.org/10.1038/475174c, 2011.

Lyu, Y., Zheng, S., Tan, G. and Shu, C.: Effects of Three Gorges Dam operation on spatial distribution and evolution of channel thalweg in the Yichang-Chenglingji Reach of the Middle Yangtze River, China, J. Hydrol., 565, 429-442, https://doi.org/10.1016/j.jhydrol.2018.08.042, 2018.

Mei, X., Dai, Z., Gelder, P.H.A.J. and Gao, J.: Linking Three Gorges Dam and downstream hydrological regimes along the Yangtze River, China, Earth Space Sci., 2(4), 94-106, https://doi.org/10.1002/2014EA000052, 2015a.

Mei, X., Dai, Z., Du, J. and Chen, J.: Linkage between Three Gorges Dam impacts and the dramatic recessions in China's largest freshwater lake, Poyang Lake, Sci. Rep., 5,18197, https://doi.org/10.1038/srep18127, 2015b.

Nakayama, T., and Shankman, D.: Impact of the Three-Gorges Dam and water transfer project on Changjiang floods, Global Planet Change, 100, 38-50, https://doi.org/10.1016/j.gloplacha.2012.10.004, 2013.

Qiu, C. and Zhu., J.: Influence of seasonal runoff regulation by the Three Gorges Reservoir on saltwater intrusion in the Changjiang River Estuary, Cont. Shelf Res., 71,

16-26, https://doi.org/10.1016/j.csr.2013.09.024, 2013.

Rahman, M., Dustegir, M., Karim, R., Haque, A., Nicholls, R. J., Darby, S. E., Nakagawa, H., Hossain, M., Dunn, F. E., and Akter, M.: Recent sediment flux to the Ganges-Brahmaputra-Meghna delta system, Sci. Total Environ., 643, 1054-1064, https://doi.org/10.1016/j.scitotenv.2018.06.147, 2018.

Räsänen, T. A., Someth, P., Lauri, H., Koponen, J., Sarkkula, J., and Kummu, M.: Observed river discharge changes due to hydropower operations in the Upper Mekong Basin, J. Hydrol., 545, 28-41, https://doi.org/10.1016/j.jhydrol.2016.12.023, 2017.

Sassi, M. G., and Hoitink, A. J. F.: River flow controls on tides and tide-mean water level profiles in a tidal freshwater river, J. Geophys. Res., 118(9), 4139-4151, https://doi.org/10.1002/jgrc.20297, 2013.

Savenije, H. H. G.: Salinity and Tides in Alluvial Estuaries, Elsevier, New York, USA, 2005.

Savenije, H. H. G.: Salinity and Tides in Alluvial Estuaries (2nd completely revised edition), Available at www.salinityandtides.com (Last access: 10 December 2018), 2012.

Savenije, H. H. G., Toffolon, M., Haas, J., and Veling, E. J. M.: Analytical description of tidal dynamics in convergent estuaries, J. Geophys. Res., 113, C10025, https://doi.org/10.1029/2007JC004408, 2008.

Shaikh, B.Y., Bansal, R.K., Das, S.K.: Propagation of Tidal Wave in Coastal Terrains with Complex Bed Geometry, Environmental Processes, 5(3), 519-537, https://doi.org/10.1007/s40710-018-0314-7, 2018.

Shi, S., Cheng, H., Xuan, X., Hu, F., Yuan, X., Jiang, Y., and Zhou, Q.: Fluctuations in the tidal limit of the Yangtze River estuary in the last decade, Sci. China Earth Sci., 61 (8), 1136-1147, https://doi.org/10.1007/s11430-017-9200-4, 2018.

Wang, Y., Ridd, P.V., Wu, H., Wu, J. and Shen, H.: Long-term morphodynamic evolution and the equilibrium mechanism of a flood channel in the Yangtze Estuary (China), Geomorphology, 99(1-4), 130-138, https://doi.org/10.1016/j.geomorph.2007.10.003, 2008.

Vignoli, G., Toffolon, M., and Tubino, M.: Non-linear frictional residual effects on tide propagation, in, Proceedings of IAHR Congress, vol. A, 24-29 August 2003, Thessaloniki, Greece, 291-298, 2003.

Zhang, E. F., Savenije, H. H. G., Chen, S. L., and Mao, X. H.: An analytical solution for tidal propagation in the Yangtze Estuary, China, Hydrol. Earth Syst. Sci., 16(9), 3327-3339, https://doi.org/10.5194/hess-16-3327-2012, 2012.

Zhang, F., Sun, J., Lin, B., and Huang, G.: Seasonal hydrodynamic interactions between tidal waves and river flows in the Yangtze Estuary, J. Marine Syst., 186, 17-28, https://doi.org/10.1016/j.jmarsys.2018.05.005, 2018.

Zhang, M., Townend, I., Cai, H., and Zhou, Y.: Seasonal variation of tidal prism and energy in the Changjiang River estuary: A numerical study, Chin. J. Oceanol. Limn., 34 (1), 219-230, https://doi.org/10.1007/s00343-015-4302-8, 2015a.

Zhang, M., Townend, I., Cai, H., and Zhou, Y.: Seasonal variation of river and tide energy in the Yangtze estuary, China, Earth Surf. Proc. Land., 41(1): 98-116, https://doi.org/10.1002/esp.3790, 2015b.

Zhao, T., Zhao, J., Yang, D. and Wang, H.: Generalized martingale model of the uncertainty evolution of streamflow forecasts, Adv. Water Resour., 57, 41-51, https://doi.org/10.1016/j.advwatres.2013.03.008, 2013.

**Appendix A. Simplified momentum balance for the residual water level slope**

Assuming a periodic variation of flow velocity, the integration of Equation (1) over a tidal cycle leads to an expression for the residual water level slope (e.g. Cai et al., 2014a, 2016):

$$\frac{\partial \overline{Z}}{\partial x} = -\frac{1}{K^2}\overline{\left(\frac{U|U|}{h^{4/3}}\right)} - \frac{1}{2g}\frac{\partial \overline{U^2}}{\partial x} - \frac{1}{2\rho_0}\overline{h\frac{\partial \rho}{\partial x}} \tag{8}$$

where the overbars and the subscript 0 indicate the tidal average and value at the seaward boundary, respectively. The residual water level slope is induced by three contributions: residual frictional, advective acceleration, and density effects, which correspond to the three terms on the right-hand side of Equation (8). Note that the contribution from advective acceleration to the residual water level slope:

$$\frac{\partial \overline{Z}_{adv}}{\partial x} = -\frac{1}{2g}\frac{\partial \overline{U^2}}{\partial x}, \tag{9}$$

can be easily integrated to:

$$\overline{Z}_{adv} = -\frac{1}{2g}\left(\overline{U^2} - \overline{U_0^2}\right) = -\frac{1}{2}\overline{Fr_0}\left(\frac{\overline{U^2}}{\overline{U_0^2}} - 1\right)\overline{h_0} \tag{10}$$

where the Froude number is introduced, $\overline{Fr^2} = \overline{U^2}/(g\overline{h})$, which is computed with the averaged variables. In this case, the correction is local (not cumulative) and proportional to the flow depth through a coefficient that is negligible as long as the velocity does not change significantly, and $Fr$ is small, as is common in most tidal flows.

787     It was shown by Savenije (2005, 2012) that the density term in equation (1) always

788     exercises a pressure in the landward direction, which is counteracted by a residual water

789     level slope, amounting to 1.25% of the estuary depth over the salt intrusion length. The

790     value for the residual water level slope, induced by the density effect, is usually small

791     compared with the gradient of the free surface elevation; thus, in this paper, we neglect

792     the influence of the density difference on the dynamics of the residual water level.

793

794     **Appendix B. Governing equations for tide-river dynamics in estuaries**

795     The analytical solutions for the dependent parameters $\mu$, $\delta$, $\lambda$, and $\varepsilon$ are obtained by

796     solving the following four dimensionless equations (see details in Cai et al., 2014a):

797     the tidal damping/amplification equation, describing the tidal amplification or damping

798     as a result of the balance between channel convergence $(gq)$ and bottom friction

799     $(cm/G)$:

$$\delta = \frac{\mu^2 \left( \gamma\theta - \chi\mu\lambda\Gamma \right)}{1 + \mu^2\beta}, \tag{11}$$

801     the scaling equation, describing how the ratio of velocity amplitude to tidal amplitude

802     depends on phase lag and wave celerity:

$$\mu = \frac{\sin(\varepsilon)}{\lambda} = \frac{\cos(\varepsilon)}{\gamma - \delta}, \tag{12}$$

804     the celerity equation, describing how the wave celerity depends on the balance between

805     convergence and tidal damping/amplification:

$$\lambda^2 = 1 - \delta(\gamma - \delta), \tag{13}$$

807     and the phase lag equation, describing how the phase lag between HW and HWS

808     depends on wave celerity, convergence, and damping:

809
$$\tan(\varepsilon) = \frac{\lambda}{\gamma - \delta}, \tag{14}$$

810 where $q$, $b$, and $G$ account for the effect of river discharge and where:

811 $$\beta = \theta - r_s\zeta\varphi/(\mu\lambda), \quad \theta = 1 - \left(\sqrt{1+\zeta} - 1\right)\varphi/(\mu\lambda), \quad \Gamma = \frac{1}{\pi}\left[p_1 - 2p_2\varphi + p_3\varphi^2\left(3 + \mu^2\lambda^2/\varphi^2\right)\right].$$

812 $$\tag{15}$$

813 Note that $\Gamma$ is a friction factor obtained by using Chebyshev polynomials (Dronkers,

814 1964) to represent the non-linear friction term in the momentum equation:

815 $$F = \frac{U|U|}{K^2\overline{h}^{4/3}} \approx \frac{1}{K^2\overline{h}^{4/3}}\frac{1}{\pi}\left(p_0\upsilon^2 + p_1\upsilon U + p_2 U^2 + p_3 U^3/\upsilon\right) \tag{16}$$

816 in which $U$ is the cross-sectional averaged velocity consisting of a steady component

817 $U_r$, generated by the fresh water discharge, and a time-dependent component $U_t$,

818 introduced by the tide:

819 $$U = U_t - U_r = \upsilon\sin(\omega t) - Q/\overline{A} \tag{17}$$

820 where $Q$ is the fresh water discharge (treated as a constant during the tidal wave

821 propagation), and $p_i$ ($i$= 0, 1, 2, 3) are the Chebyschev coefficients (see Dronkers, 1964,

822 p. 301), which are functions of the dimensionless river discharge $\varphi$ through $\alpha$ = arcos(-

823 $\varphi$):

824 $$p_0 = -\frac{7}{120}\sin(2\alpha) + \frac{1}{24}\sin(6\alpha) - \frac{1}{60}\sin(8\alpha), \tag{18}$$

825 $$p_1 = \frac{7}{6}\sin(\alpha) - \frac{7}{30}\sin(3\alpha) - \frac{7}{30}\sin(5\alpha) + \frac{1}{10}\sin(7\alpha), \tag{19}$$

826 $$p_2 = \pi - 2\alpha + \frac{1}{3}\sin(2\alpha) + \frac{19}{30}\sin(4\alpha) - \frac{1}{5}\sin(6\alpha), \tag{20}$$

827 $$p_3 = \frac{4}{3}\sin(\alpha) - \frac{2}{3}\sin(3\alpha) + \frac{2}{15}\sin(5\alpha). \tag{21}$$

828 The coefficients $p_1$, $p_2$, and $p_3$ determine the magnitudes of the linear, quadratic, and

829 cubic frictional interaction, respectively.

830